IEEE Access
Multidisciplinary | Rapid Review | Open Access Journal

Received December 12, 2019, accepted December 28, 2019, date of publication January 6, 2020, date of current version January 10, 2020.

Digital Object Identifier 10.1109/ACCESS.2020.2964035

Fingerprint Enhancement Based on Tensor of Wavelet Subbands for Classification

NGOC TUYEN LE[1], JING-WEIN WANG[1], DUC HUY LE[1], CHIH-CHIANG WANG[2], AND TU N. NGUYEN[3], (Senior Member, IEEE)

[1]Institute of Photonics Engineering, National Kaohsiung University of Science and Technology, Kaohsiung 80778, Taiwan
[2]Department of Computer Science and Information Engineering, National Kaohsiung University of Science and Technology, Kaohsiung 80778, Taiwan
[3]Department of Computer Science, Purdue University Fort Wayne, Fort Wayne, IN 46805, USA

Corresponding author: Jing-Wein Wang (jwwang@nkust.edu.tw)

This work was supported in part by the Ministry of Science and Technology, Taiwan, under Grant MOST 107-2218-E-992-310.

ABSTRACT Fingerprint image enhancement is a key aspect of an automated fingerprint identification system. This paper describes an effective algorithm based on a novel lighting compensation scheme. The scheme involves the use of adaptive higher-order singular value decomposition on a tensor of wavelet subbands of a fingerprint (AHTWF) image to enhance the quality of the image. The algorithm consists of three stages. The first stage is the decomposition of an input fingerprint image of size $2M \times 2N$ into four subbands at the first level by applying a two-dimensional discrete wavelet transform. In the second stage, we construct a tensor in $\mathbb{R}^{M\times N\times 4}$ space. The tensor contains four wavelet subbands that serve as four frontal planes. Furthermore, the tensor is decomposed through higher-order singular value decomposition to separate the fingerprint's wavelet subbands into detailed individual components. In the third stage, a compensated image is produced by adaptively obtaining the compensation coefficient for each frontal plane of the tensor-based on the reference Gaussian template. The experimental results indicated that the quality of the AHTWF image was higher than that of the original image. The proposed algorithm not only improves the clarity and continuity of ridge structures but also removes the background and blurred regions of a fingerprint image. Therefore, this algorithm can achieve higher fingerprint classification accuracy than related methods can.

INDEX TERMS Tensor, discrete wavelet transform, fingerprint classification, fingerprint enhancement, singular value decomposition.

I. INTRODUCTION

Fingerprint classification is a required preliminary step in automated fingerprint identification systems (AFIS), which are increasingly used in law enforcement agencies to identify criminals as well as in commercial, civilian, philological, and financial domains. Fingerprint classification considerably reduces the identification time of an AFIS, for which accuracy and speed are critical. Most fingerprint classification algorithms are used to classify fingerprints into four or five classes, as described by Henry [1]. In [2], fingerprints were classified into seven classes according to hierarchical singular point detection and traced orientation flow. In this method, fingerprints were divided into seven classes by separating Whorls into three types: Eddy (E), S-type (S), and Whorl. Most fingerprint classification methods are based on one or more of the following features: image orientation, ridgeline flow, singular points, and Gabor filter responses [2]–[7]. The performance of each method depends considerably on the quality of the fingerprint image. A low-quality fingerprint image leads to adequate or false feature extraction (in terms of aspects such as minutiae and singular points). Therefore, fingerprint image enhancement is a key step in an AFIS. Before being input into an AFIS, a fingerprint image must undergo an enhancement stage that removes overlapping patterns, connects broken ridges, and separates joined ridges. Fingerprint image enhancement has been investigated in multiple ongoing and completed studies. Researchers have attempted to reduce noise and improve the contrast between ridges and valleys in fingerprint images. Generally, methods of enhancement can be broadly divided into three categories: filtering methods, model-based methods, and multiresolution methods.

Filtering methods are those that use filters to enhance a fingerprint image. Wang and Wang [8] initially detected a singular point area and then enhanced this area by applying

The associate editor coordinating the review of this manuscript and approving it for publication was Gulistan Raja.

a bandpass filter in the Fourier domain. However, detecting a singular point region is very difficult when the quality of the fingerprint image is extremely poor. The Log-Gabor filter, which was introduced by Wang *et al.* [9], is used for fingerprint enhancement; however, the logarithm function is nonlinear, which leads to a loss of dominant information in fingerprint images. Gottschlich [10] introduced curved Gabor filters (cGFs) to enhance curved structures in noisy fingerprint images. This cGFs are defined on the basis of curved regions and then applied to previously estimated orientations and ridge frequencies for the enhancement of low-quality fingerprint images.

Model-based methods are those that attempt to extract features from fingerprint images and then use them for modeling or learning before reconstruction to obtain enhanced images. Jirachaweng *et al.* [12] used multiple Legendre polynomials to determine the global orientation pattern of a fingerprint image and reconstruct the orientation field according to the structure of the fingerprint. They then enhanced the image by using gradient estimation. Yun and Cho [13] analyzed fingerprint images, divided them into three types—oily, neutral, and dry—according to their properties, and then applied a specific enhancement strategy for each type. Cao and Jain [14] applied prior knowledge of fingerprint ridge structures to encode orientation patch and continuous phase patch dictionaries and to facilitate fingerprint reconstruction. The orientation patch dictionary was used to reconstruct an orientation field from minutiae, whereas the continuous phase patch dictionary was used to reconstruct the ridge pattern.

Multiresolution methods attempt to decompose a fingerprint image into multiple frequency subbands and allow compensation for noise components on various scales. To enhance a fingerprint image, Fronthaler *et al.* [15] used a Laplacian-like image pyramid to decompose an original image into subbands corresponding to multiple spatial scales. They then performed contextual smoothing on these pyramidal scales, where the corresponding filtering directions were determined by a frequency-adapted structure tensor. Lei *et al.* [16] initially decomposed a fingerprint image by using non-separable filter banks to obtain wavelet coefficients. They subsequently modified these coefficients through an adaptive approach to reduce noise and increase the contrast between ridges and valleys according to the geometric features of the image. Hsieh *et al.* [17] decomposed a normalized fingerprint image by using wavelet transform and then applied global texture filtering to remove spectral and textural noise. Subsequently, local directional compensation based on a set of 16 predefined directional masks was applied to wavelet coefficients. Notably, the selection of predefined mean and variance values used to normalize a fingerprint image is heuristic. Bennet and Perumal [18] enhanced a fingerprint image by multiplying the singular value matrix of a low subband by the ratio of the largest singular value of a generated normalized matrix with a mean of 0 and variance of 1 to the largest singular value of the low subband. Parts of the resultant images were uneven because singular value decomposition (SVD) was applied in only the LL subband and a generated normalized matrix was used. To overcome this problem, Wang *et al.* [19] introduced a novel lighting compensation scheme involving the use of adaptive SVD on wavelet coefficients. First, an input fingerprint image was decomposed into four subbands through a two-dimensional discrete wavelet transform (2D-DWT). Subsequently, the image was compensated for by adaptively obtaining the compensation coefficients for each subband based on a reference Gaussian template. However, in this method, SVD was applied in each wavelet subband individually. Thus, the method was unable to identify relationships among subbands. Consequently, some results were not as expected.

Over the past two decades, the use of tensors and their decomposition has become increasingly popular. In multilinear algebra, higher-order SVD (HOSVD) of a tensor is a specific orthogonal Tucker decomposition [20]–[22]. The power of a tensor framework can be presented in a visually and mathematically compelling manner by decomposing and representing an image in terms of its causal factors with respect to data formation. HOSVD has been successfully applied to signal processing as well as big data [23]–[25], computer vision [26], and facial recognition [27]–[31].

This paper introduces a novel algorithm for fingerprint image enhancement. The introduced algorithm is based on a novel lighting compensation scheme that involves the use of adaptive HOSVD on a tensor of wavelet subbands. The algorithm has three stages. The first stage involves the decomposition of an input fingerprint image sized $2M \times 2N$ into four subbands at the first level through the application of 2D-DWT. In the second stage, a tensor is constructed in $\mathbb{R}^{M \times N \times 4}$ space. This tensor contains four wavelet subbands that serve as four frontal planes. The tensor is then decomposed through HOSVD to separate the fingerprint's wavelet subbands into detailed individual components. In the third stage, a compensated image is produced by adaptively obtaining the compensation coefficient for each frontal plane of the tensor and fixing its inverse factor U_3 according to the reference Gaussian template. The experimental results indicated that the quality of the compensated image was higher than that of the original image. Thus, the proposed algorithm can not only improve the clarity and continuity of ridge structures but can also remove the background of a fingerprint image. Therefore, the proposed algorithm can attain higher fingerprint classification rates than related methods can. The experimental results for the National Institute of Standards and Technology (NIST)-4 [32] and Fingerprint Verification Competition (FVC) 2002 [33] databases indicate that the proposed method can substantially improve the clarity and continuity of ridge structures. In addition, this method can effectively remove the background of a fingerprint image and minimize the blurred regions in it. This study achieved a relatively high singular point detection rate. Thus, a higher fingerprint classification rate was achieved with the proposed method than with related methods.

The remainder of the paper is organized as follows. Section II introduces 2D-DWT applied to the fingerprint image. Section III introduces the HOSVD of a tensor. Section IV describes the proposed algorithm. The experimental results are reported in Section V, and the conclusion is presented in Section VI.

II. WAVELET TRANSFORM OF A FINGERPRINT IMAGE

2D-DWT is used extensively in digital image processing [19], [34], [35]. In the present study, DWT involved transformation from the spatial domain into the wavelet domain. DWT based on the octave-band tree structure can be viewed as the multiresolution decomposition of a signal. In two-band wavelet transform, the signal $f(x)$ can be expressed by wavelet and scaling basis functions on different scales in a hierarchical manner:

$$f(x) = \sum_{k} c_{j_0(k)} \varphi_{j_0,k}(x) + \sum_{j=0}^{\infty} \sum_{k} d_j(k)\, \psi_{j,k}(x), \quad (1)$$

where j_0 is an arbitrary initial scale; $\varphi_{j_0,k}$ and $\psi_{j,k}$ are the scaling function and wavelet function at scale j, respectively; $c_{j_0(k)}$ is an approximation of the scaling coefficient; and $d_j(k)$ is the detailed wavelet coefficient. 2D-DWT is represented in terms of translations and dilations of the scaling and wavelet functions, which can be computed using a 2D filter bank consisting of low- and high-pass filters.

Consider the following scaled and translated basis functions:

$$\varphi_{j,m,n}(x,y) = 2^{j/2} \varphi\left(2^j x - m, 2^j y - n\right), \quad (2)$$

$$\psi^i_{j,m,n}(x,y) = 2^{j/2} \psi\left(2^j x - m, 2^j y - n\right), \quad (3)$$

where the index $i = \{H, V, D\}$ denotes the horizontal, vertical, and diagonal directional wavelets, respectively. 2D-DWT of image $f(x, y)$ of size $M \times N$ is expressed as follows:

$$W_\varphi(j_0, m, n) = \frac{1}{\sqrt{MN}} \sum_{x=0}^{M-1} \sum_{y=0}^{N-1} f(x,y)\, \varphi_{j_0,m,n}(x,y), \quad (4)$$

$$W^i_\psi(j, m, n) = \frac{1}{\sqrt{MN}} \sum_{x=0}^{M-1} \sum_{y=0}^{N-1} f(x,y)\, \psi^i_{j,m,n}(x,y), \quad (5)$$

where $i = \{H, V, D\}$, and the $W_\varphi(j_0, m, n)$ coefficients define an approximation of $f(x, y)$ at scale j_0. The $W^i_\psi(j, m, n)$ coefficients add horizontal, vertical, and diagonal details for the scale $j \geq j_0$. After 2D-DWT decomposition, the given image is decomposed into several multiresolution frequency components, as displayed in Fig. 1. The subbands HH_j, HL_j, LH_j, $j = 1, \ldots, J$, are referred to details, with J being the largest scale in the decomposition. A subband at scale j has the size $M/2^j \times N/2^j$. The subband LL_J is the low-resolution residual, and J is typically sufficiently large so that $M/2^J \ll M, N/2^J \ll N$ and $\min\left(M/2^J, N/2^J\right) > 1$.

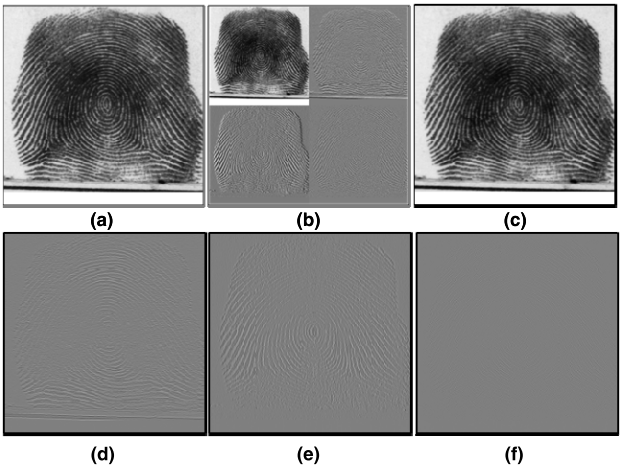

FIGURE 1. 2D-DWT of a fingerprint image. (a) Fingerprint image in the NIST-4 database. (b) Four subbands after the use of 2D-DWT at the first level. (c) Image reconstructed using only the LL subband coefficients (the remaining coefficients were set to 0). (d) Image reconstructed using only the LH subband coefficients (the remaining coefficients were set to 0). (e) Image reconstructed using only the LH subband coefficients (the remaining coefficients were set to 0). (f) Image reconstructed using only the HH subband coefficients (the remaining coefficients were set to 0).

In accordance with W_φ and W^i_ψ in Eqs. (4) and (5), $f(x, y)$ is obtained through inverse 2D-DWT (2D-iDWT) as follows:

$$\begin{aligned} f(x,y) &= \frac{1}{\sqrt{MN}} \sum_{m} \sum_{n} W_\varphi(j_0, m, n)\, \varphi_{j_0,m,n}(x,y) \\ &\quad + \frac{1}{\sqrt{MN}} \sum_{i=\{H,V,D\}} \sum_{j=j_0}^{\infty} \sum_{m} \sum_{n} W^i_\psi(j, m, n)\, \psi^i_{j,m,n}(x,y). \end{aligned} \quad (6)$$

Wavelet transform is a multiresolution image decomposition tool that can represent image features through various frequency subbands on multiple scales. Therefore, this tool has the well-known advantage of multiscale analysis. Moreover, the wavelet transform has the compaction property of only a small number of large coefficients due to key signal features. The small coefficients are primarily the result of noise. Moreover, noise is averaged to almost zero in the low-frequency wavelet coefficients, all of which are sensitive to illumination. Thus, only the wavelet coefficients in the mid- and high-frequency subbands are thresholded to remove noise. Fig. 1 depicts 2D-DWT with Daubechies mother wavelet function of a fingerprint image at the first level and images reconstructed using only the coefficients of one of the four subbands; the remaining coefficients were set to 0. As displayed in Fig. 1(c), most of the dominant information in the fingerprint images were obtained in the low-frequency subband. Information on ridge structures was obtained in the mid-frequency subbands [Fig. 1(d) and (e)], and the noise distribution was obtained from the high-frequency subband [Fig. 1(f)]. We analyze the relevance of the aforementioned wavelet subbands and then apply adaptively linear changes to

them before using 2D-iDWT to obtain enhanced fingerprint images.

III. WAVELET SUBBANDS OF A FINGERPRINT IMAGE AS A TENSOR AND ITS HOSVD

A. TENSOR FUNDAMENTALS

This subsection provides an overview of fundamental tensor concepts and methods of extracting key information from tensors by using HOSVD. For uniformity among symbols, the matrix is denoted by an italic capital letter (e.g., "A") and the tensor is denoted by a boldface Euler script letter (e.g., "$\mathcal{A}$"). The formal definitions are given as follows [36].

Definition 1: A tensor is a multidimensional array. In formal terms, an N-way or N^{th}-order tensor is an element of the tensor product of N vector spaces, each of which has its own coordinate system.

Definition 2: The order of a tensor is the number of dimensions, which are also known as ways or modes.

Definition 3: The fibers are the higher-order analogue of matrix rows and columns. A fiber is defined by fixing every index but one. A matrix column is a mode-1 fiber, and a matrix row is a mode-2 fiber. Third-order tensors have column, row, and tube fibers, which are denoted by $a_{:\mathrm{jk}}$, $a_{\mathrm{i}:\mathrm{k}}$, and $a_{\mathrm{ij}:}$, respectively. When extracted from a tensor, fibers are always assumed to be oriented as column vectors.

Definition 4: Slices are 2D sections of a tensor defined by fixing all but two indices. A third-order tensor $\mathcal{A} \in \mathbb{R}^{\mathrm{I}_1 \times \mathrm{I}_2 \times \mathrm{I}_3}$ includes horizontal, lateral, and frontal slices denoted by $A_{\mathrm{i}::}$, $A_{:\mathrm{j}:}$, and $A_{::\mathrm{k}}$, respectively. Alternatively, the k^{th} frontal slice of a third-order tensor, $A_{::\mathrm{k}}$, is denoted concisely as A_{k}, $k = 1, 2, \ldots, I_3$.

Definition 5: The mode-k unfolding of a tensor $\mathcal{A} \in \mathbb{R}^{\mathrm{I}_1 \times \mathrm{I}_2 \times \cdots \times \mathrm{I}_{\mathrm{N}}}$ is denoted by $A_{(\mathrm{k})}$, which arranges the mode-k fibers as columns of the resultant matrix.

Unfolding, which is also known as matricization or flattening, is the process of reordering the elements of an N-way array into a matrix. Although the process is conceptually simple, its formal notation is clunky. The tensor element $(I_1 \times I_2 \times \cdots \times I_N)$ maps to the matrix element (i, j), where

$$j = 1 + \sum_{\substack{k=1 \\ k \neq n}}^{N} (i_k - 1)\, J_k \text{with } J_k = \prod_{\substack{m=1 \\ m \neq n}}^{k-1} I_m. \tag{7}$$

Definition 6: The mode-k (matrix) product of a tensor $\mathcal{A} \in \mathbb{R}^{I_1 \times I_2 \times \cdots \times I_N}$ with a matrix $U \in \mathbb{R}^{J \times I_N}$ is denoted by $\mathcal{A} \times_{\mathrm{k}} U$ and is of size $I_1 \times \cdots \times I_{k-1} \times J \times I_k \times \cdots \times I_N$. In terms of elements, we obtain the following expression:

$$(\mathcal{A} \times_k U)_{i_1 \cdots i_{k-1} j i_k \cdots i_N} = \sum_{i_k=1}^{I_K} a_{i_1 i_2 \cdots i_N} u_{j i_k}. \tag{8}$$

Each mode-k fiber is multiplied by the matrix U. This idea can be expressed in terms of unfolded tensors as follows:

$$\mathcal{A} = \mathcal{X} \times_k U \Leftrightarrow A_{(k)} = U X_{(k)}. \tag{9}$$

Definition 7: The HOSVD of a tensor $\mathcal{A} \in \mathbb{R}^{\mathrm{I}_1 \times \mathrm{I}_2 \times \cdots \times \mathrm{I}_{\mathrm{N}}}$ is expressed as follows:

$$\mathcal{A}(i_1, i_2, \ldots, i_N) = \sum_{j_1=1}^{I_1} \cdots \sum_{j_N=1}^{I_N} \mathcal{S}(j_1, j_2, \ldots, j_N) . U_1(i_1, j_1) \ldots U_N(i_N, j_N), \tag{10}$$

or

$$\mathcal{A} = \mathcal{S} \times_1 U_1 \times_2 U_2 \ldots \times_N U_N, \tag{11}$$

where tensor $\mathcal{S} \in \mathbb{R}^{I_1 \times I_2 \times \cdots \times I_N}$ is the core tensor and matrices $U_1 \in \mathbb{R}^{I_1 \times I_1}, U_2 \in \mathbb{R}^{I_2 \times I_2}, \ldots, U_N \in \mathbb{R}^{I_N \times I_N}$ are inverse factors. When the order of a tensor is 3, Eq.(11) is an "illumination" Tucker product representation of $\mathcal{A}$.

Considering that $A_{(k)}$ denotes the mode-k unfolding of the tensor $\mathcal{A}$, $S_{(k)}$ denotes the mode-k unfolding of the core tensor $\mathcal{S}$. The SVD of $A_{(k)}$ is expressed as follows:

$$A_{(k)} = U_k \Sigma_k V_k^T, \tag{12}$$

Subsequently, $S_{(k)}$ is calculated as follows:

$$S_{(k)} = \Sigma_k V_k (U_N \otimes \cdots \otimes U_{k+1} \otimes U_{k-1} \otimes \cdots \otimes U_1), \tag{13}$$

or

$$\mathcal{S} = \mathcal{A} \times_1 U_1^T \times_2 U_2^T \ldots \times_N U_N^T, \tag{14}$$

and tensor $\mathcal{A}$ is represented in the form of unfolding as follows:

$$A_{(k)} = U_k S_{(k)} (U_N \otimes \cdots \otimes U_{k+1} \otimes U_{k-1} \otimes \cdots \otimes U_1)^T, \tag{15}$$

where $\otimes$ denotes the Kronecker product of the matrices.

B. TENSOR OF THE WAVELET SUBBANDS OF A FINGERPRINT IMAGE

To effectively exploit the relationship between the wavelet subbands of the fingerprint image, we construct a tensor with four frontal slices denoting four wavelet subbands. The wavelet subbands of the fingerprint image are represented by a third-order tensor defined by two indices for spatial variables and one index for the wavelet subband mode. Mode-1 of the tensor is the height of a wavelet subband, mode-2 is the width of a wavelet subband, and mode-3 represents the wavelet subbands of the fingerprint image. For example, a fingerprint image of size $2M \times 2N$ is transformed through 2D-DWT at scale level 1. Thus, the tensor of the wavelet subbands of the fingerprint image is expressed as a third-order tensor $\mathcal{A} \in \mathbb{R}^{M \times N \times 4}$ space, as displayed in Fig. 2(a), where M and N correspond to the v-resolution (vertical) and h-resolution (horizontal), respectively, and the number of wavelet subbands is 4.

Without loss of generality, the four frontal slices of $\mathcal{A}$ are denoted by A_i, $i = 1, 2, 3, 4$ and the three mode-k unfolding matrices, $k = 1, 2, 3$, are denoted by $A_{(k)}$. According to Definition 7, the "illumination" Tucker product representation of $\mathcal{A}$ can be expressed as follows:

$$\mathcal{A} = \mathcal{S} \times_1 U_1 \times_2 U_2 \times_3 U_3, \tag{16}$$

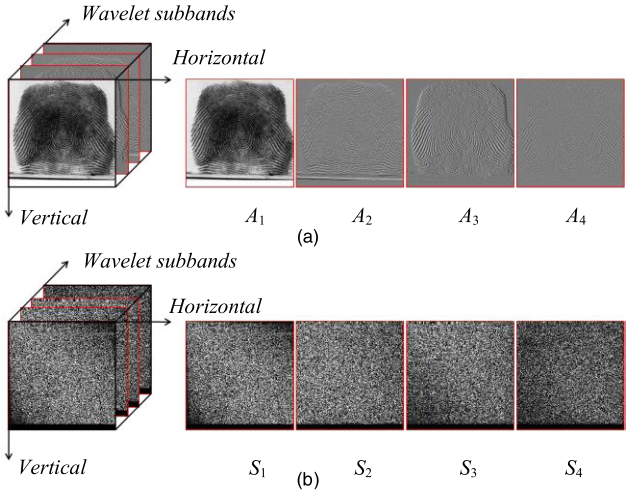

FIGURE 2. (a) Four wavelet subbands ordered in the third-order tensor $\mathcal{A} \in \mathbb{R}^{M\times N\times 4}$ space. The tensor has four frontal slices, where the first frontal slice is LL subband, the second frontal slice is LH subband, the third frontal slice is LL subband, and the fourth frontal slice is HH subband. (b) The core tensor of (a) after applying HOSVD.

where $U_i, i = 1, 2, 3$ are the inverse factors of $\mathcal{A}$ and $\mathcal{S}$ is the core of tensor $\mathcal{A}$. Thereafter, we denote the four frontal slices of $\mathcal{S}$ by $S_{\rm i}$, $i = 1, 2, 3, 4$ and the three mode-k unfolding matrices of $\mathcal{S}$ by $S_{\rm (k)}$, $k = 1, 2, 3$. In this study, the frontal slices $A_{\rm i}$ and $S_{\rm i}$ are matrices of size $M\times N$, the mode-1 unfolding matrices $A_{(1)}$ and $S_{(1)}$ are matrices of size $M\times(4N)$, the mode-2 unfolding matrices $A_{(2)}$ and $S_{(2)}$ are matrices of size $N\times(4M)$, the mode-3 unfolding matrices $A_{(3)}$ and $S_{(3)}$ are matrices of size $3\times(MN)$, and the inverse factors $U_i, i = 1, 2, 3$ are square matrices of size $r_i \times r_i$, with $r_i = \text{rank}(U_i)$. The core tensor $\mathcal{S}$ and its frontal slices are depicted in Fig. 2(b). In contrast to SVD, the core coefficients are not only located on the main diagonal of the frontal slices but are also evenly distributed across the slices. However, large values are also distributed around the main diagonal lines.

To analyze whether each component of HOSVD [right side of Eq. (16)] carries specific information of the fingerprint image, we alternately replace the core $\mathcal{S}$ with the identity tensor and replace the inverse factors $U_i, i = 1, 2, 3$ with the respective identity matrices. The identity tensor is a tensor in which all frontal slices serve as the identity matrices. The new wavelet subbands received from the reconstructed tensor are used to rebuild the fingerprint image through 2D-iDWT.

Fig. 3(a) displays two fingerprint images with different sizes and different backgrounds from the FVC 2002 database. The first row displays an image in the DB1-A database with a white background measuring 388×374 pixels. The second row displays an image in the DB3-A database with a gray background measuring 300×300 pixels. Fig. 3(b) illustrates the resultant fingerprint image after the core $\mathcal{S}$ is replaced with the identity tensor. Fig. 3(c) depicts the resultant fingerprint image after the inverse factor U_1 is replaced with the identity matrix. Fig. 3(d) shows the resultant fingerprint image after the inverse factor U_2 is replaced with the identity matrix. Fig. 3(e) illustrates the resultant fingerprint image after the inverse factor U_3 is replaced with the identity matrix. As displayed in Fig. 3(b), without the effect of the core tensor, the structure of the fingerprint is destroyed. Therefore, the core tensor contains the most foreground ridges of the given fingerprint image's spatial structure (edge). The results in Fig. 3(c) and (d) reveal that inverse factors U_1 and U_2 contained information on illumination in the vertical and horizontal directions, respectively. As displayed in Fig. 3(e), the foreground ridges of the fingerprint image's spatial structure are not affected by inverse factor U_3, which indicates that U_3 contains the illumination of the fingerprint image. Further, there are experiments by swapping the U_3 matrices between two fingerprint images and then reconstructing the images. As shown in Fig. 3(f), even when the fingerprint images are presented in different sizes, their U_3 matrices are of the same size (4 × 4 pixels in this case). Moreover, when we swap the U_3 matrices of the two fingerprint images, their backgrounds change but their fingerprint structures remain the same. Thus, HOSVD of the wavelet subband tensor and inverse factor U_3 of a fingerprint image can be employed to enhance the ridge structure and remove noise from the background of the image. In addition, the problem of a low-contrast fingerprint image can be corrected by replacing the core of the wavelet subband tensor with the core of the wavelet subband tensor obtained from a normalized image. The mean and variance of the normalized image are calculated using the available dataset. The normalized image is called a Gaussian template.

IV. FINGERPRINT IMAGE ENHANCEMENT

According to the 2D DWT and HOSVD observations for the wavelet subband tensor on the fingerprint image, an effective algorithm is proposed to improve the fingerprint image quality. Assuming that f is a fingerprint image and Ga is a Gaussian template of size $2M \times 2N$, we apply 2D-DWT with the Daubechies mother wavelet function to decompose f and Ga into four subbands at level 1. The 2D matrices with subband wavelet coefficients are denoted by LL, HL,LH, and HH.

$$A_i = \left[a^i_{m,n}\right], \tag{17}$$

$$G_i = \left[g^i_{m,n}\right], \tag{18}$$

where A_i and G_i, $i \in \{LL, HL, LH, HH\}$ are subband names; $a^i_{m,n}$ and $g^i_{m,n}$, $i \in \{ll, hl, lh, hh\}$ are subband wavelet coefficients of fingerprint image f and the Gaussian template, respectively; and $m = 0, 1, \ldots, M-1$ and $n = 0, 1, \ldots, N-1$ are coefficient indices. We construct the tensor $\mathcal{A} \in \mathbb{R}^{M\times N\times \mathbf{4}}$ space with four frontal slices are four wavelet subbands $A_i, i \in \{LL, HL, LH, HH\}$. The tensor $\mathcal{G} \in \mathbb{R}^{M\times N\times \mathbf{4}}$ space also has four frontal slices are four wavelet subbands $G_i, i \in LL, HL, LH, HH$.

In the proposed method, the pre-compensation maximum of the coefficients for each frontal slice of $\mathcal{A}$ and $\mathcal{G}$ is calculated first. By using the maximum value as the reference

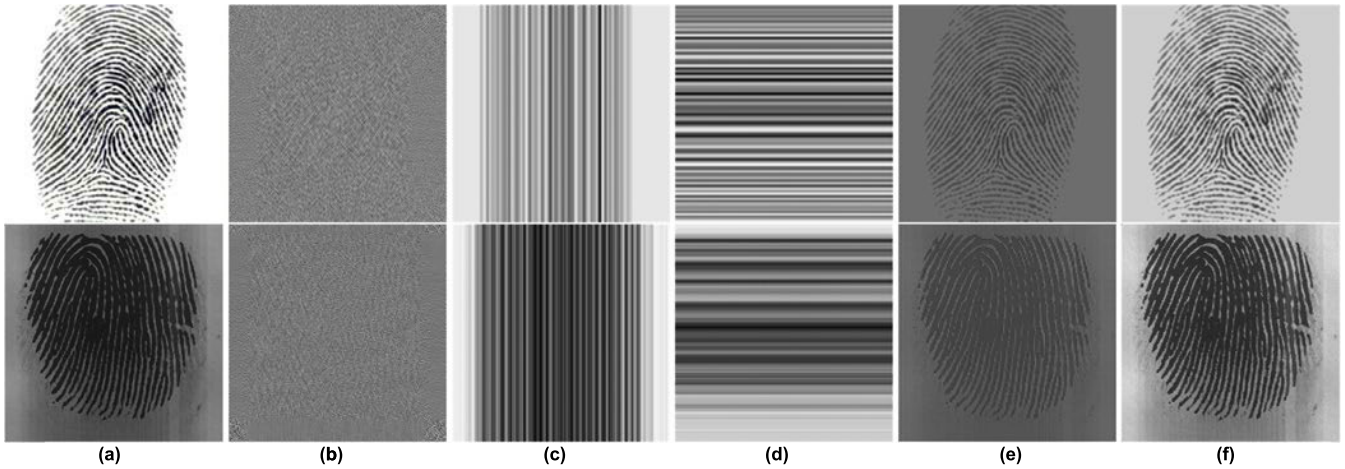

FIGURE 3. Reconstructed fingerprint images after alternate replacement of the core S by the identity tensor and the inverse factors U_i, $i = 1, 2, 3$ by the identity matrices. (a) Two fingerprint images in the FVC 2002 database. The first row shows the image in DB1-A with a white background, and the second row shows the image in DB3-A with a gray background. (b) Replacement of the core S with the identity tensor. (c) Replacement of $U1$ with the identity matrix. (d) Replacement of $U2$ with the identity matrix. (e) Replacement of $U3$ with the identity matrix. (f) Images reconstructed by swapping the $U3$ matrices of the two fingerprint images.

value, individual compensation weighting coefficients for each frontal slice are adaptively derived according to the ratio between the maxima of the frontal slices of $\mathcal{A}$ and $\mathcal{G}$. The maxima of all coefficients for all frontal slices of $\mathcal{A}$ and $\mathcal{G}$ can be calculated as follows:

$$\max_{A_i} = \max\left(a^i_{m,n}\right), \tag{19}$$

$$\max_{G_i} = \max\left(g^i_{m,n}\right). \tag{20}$$

Next, the mode-k unfolding of tensors $\mathcal{A}$ and $\mathcal{G}$ is calculated [$A_{(k)}$ and $G_{(k)}$, respectively, where $k = 1, 2, 3$]. Subsequently, the SVD of $A_{(k)}$ and $G_{(k)}$ are expressed as follows:

$$A_{(k)} = U_{A_k} \Sigma_{A_k} V^T_{A_k}, \tag{21}$$

$$G_{(k)} = U_{G_k} \Sigma_{G_k} V^T_{G_k}, \tag{22}$$

where $U_{A,k}, U_{G,k}, V_{A,k}$, and$V_{G,k}$ are orthogonal matrices with singular vectors and $\Sigma_{A,k}$ and $\Sigma_{G,k}$ contain the singular values of $A_{(k)}$ and $G_{(k)}$, respectively. $U_{A,k}$ and $U_{G,k}$ are the inverse factors of $\mathcal{A}$ and $\mathcal{G}$, respectively.

The core $\mathcal{S}$ of $\mathcal{A}$ and core $\mathcal{C}$ of $\mathcal{G}$ are calculated by mode-k unfolding $S_{(k)}$ and $C_{(k)}$, respectively, as follows:

$$S_{(1)} = \Sigma_{A_1} V_{A_1} \left(U_{A_3} \otimes U_{A_2}\right), C_{(1)} = \Sigma_{G_1} V_{G_1} \left(U_{G_3} \otimes U_{G_2}\right), \tag{23}$$

$$S_{(2)} = \Sigma_{A_2} V_{A_2} \left(U_{A_3} \otimes U_{A_1}\right), C_{(2)} = \Sigma_{G_2} V_{G_2} \left(U_{G_3} \otimes U_{G_1}\right), \tag{24}$$

$$S_{(3)} = \Sigma_{A_3} V_{A_3} \left(U_{A_2} \otimes U_{A_1}\right), C_{(3)} = \Sigma_{G_3} V_{G_3} \left(U_{G_2} \otimes U_{G_1}\right). \tag{25}$$

Subsequently, the frontal slices $S_i = (s^i_{m,n})$ and $C_i = (c^i_{m,n})$ of $\mathcal{S}$ and $\mathcal{C}$ are computed through separation from $S_{(k)}$ and $C_{(k)}$, respectively, where $m = 0, 1, \ldots, M-1$ and $n = 0, 1, 2, \ldots, N-1$. The HOSVD processes of tensors $\mathcal{A}$ and $\mathcal{G}$ are expressed as follows:

$$\mathcal{A} = \mathcal{S} \times_1 U_{A_1} \times_2 U_{A_2} \times_3 U_{A_3}, \tag{26}$$

$$\mathcal{G} = \mathcal{C} \times_1 U_{G_1} \times_2 U_{G_2} \times_3 U_{G_3}, \tag{27}$$

where $\mathcal{S}$ and $\mathcal{C}$ are the cores of tensors $\mathcal{A}$ and $\mathcal{G}$, respectively. The four frontal slices of $\mathcal{S}$ and $\mathcal{C}$ are denoted by S_i and C_i, respectively, where $i = 1, 2, 3$, and 4. The three mode-k unfolding matrices of $\mathbf{S}$ and $\mathcal{C}$ are denoted by $S_{(k)}$ and $C_{(k)}$, respectively, where $k = 1, 2, 3$.

To enhance a fingerprint image, the core tensor and inverse factor U_3 are examined. Each subband of the DWT contains distinct information related to the fingerprint image. The low-frequency subband contains most of the dominant information, the mid-frequency subbands contain most of the ridge information, and the high-frequency subband may contain noise. Moreover, we order the wavelet subbands into a tensor and then conduct HOSVD to determine the relationships among the subbands. The core of the wavelet subband tensor and its inverse factor U_3 can be used to enhance the ridge structure and remove noise from the background of a fingerprint image. We calculate the maximum of the coefficients for each frontal slice of core $\mathcal{S}$ and core $\mathcal{C}$ as follows:

$$max_{S_i} = \max\left(s^i_{m,n}\right), \tag{28}$$

$$max_{C_i} = \max\left(c^i_{m,n}\right). \tag{29}$$

Specific equations are employed to calculate the compensation coefficients of each frontal slice, which can then be used to effectively compress the dynamic range through the root function property. The compensation weight coefficients of each frontal slice are calculated as follows:

$$\xi_1 = \frac{max_{G_1}}{max_{A_1}} * \frac{max_{S_1}}{max_{C_1}}, \tag{30}$$

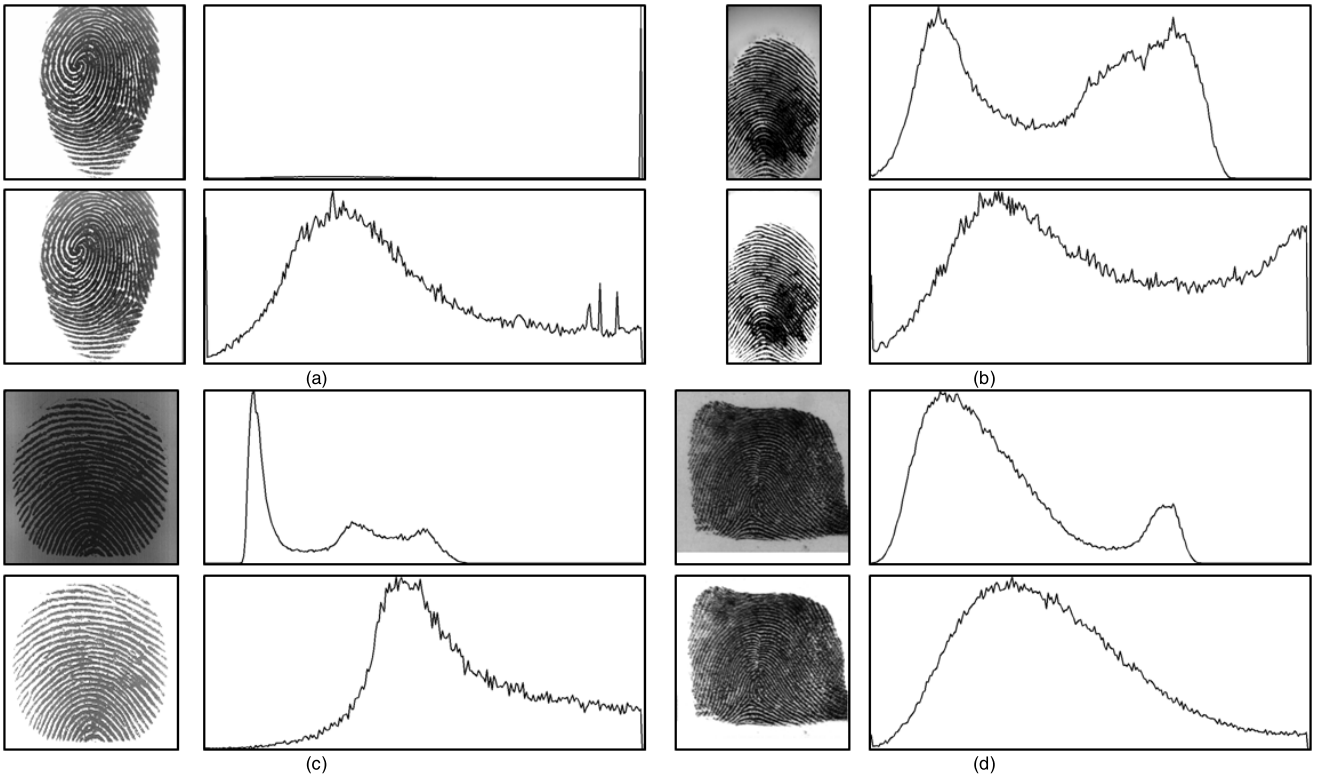

FIGURE 4. Results obtained using the proposed method. The first row shows the original fingerprint image and its histogram, and the second row shows the result of our method and its histogram. (a) FVC 2002 DB1-A, (b) FVC 2002 DB2-A, (c) FVC 2002 DB3-A, and (d) NIST-4.

$$\xi_2 = \sqrt{\frac{max_{G_2}}{max_{A_2}} * \frac{max_{S_2}}{max_{C_2}}}, \tag{31}$$

$$\xi_3 = \sqrt{\frac{max_{G_3}}{max_{A_3}} * \frac{max_{S_3}}{max_{C_3}}}, \tag{32}$$

$$\xi_4 = \frac{max_{G_4}}{max_{A_4}} * \frac{max_{S_4}}{max_{C_4}}. \tag{33}$$

where ξ_i is the compensation coefficient corresponding frontal slice i, $i = 1, 2, 3, 4$. The fingerprint contrast is adaptively adjusted by multiplying the frontal slices of core $\mathcal{S}$ by the corresponding compensation coefficients as follows:

$$S_{C_i} = \xi_i S_i. \tag{34}$$

where S_{C_i} are compensation frontal slices.

Subsequently, S_{C_i}, $i = 1, 2, 3, 4$ is used to calculate the mode-k unfolding compensation matrices $S_{C_{(k)}}$, where $k = 1, 2, 3$, for determining the compensation tensor. Inverse factor U_3 of the tensor of size 4×4 contains background information related to the fingerprint image. Therefore, we replace the inverse factor U_3 with inverse factor U_{G_3} of the Gaussian template. Each compensation tensor had the same inverse factor (U_{G_3}). According to $S_{C_{(k)}}$ and U_{G_3}, the compensation tensor ($\mathcal{A}_{\mathcal{C}}$) is calculated with one of the following three equations:

$$A_{C_{(1)}} = U_{A_1} S_{C_{(1)}} \left(U_{G_3} \otimes U_{A_2}\right)^T, \tag{35}$$

$$A_{C_{(2)}} = U_{A_2} S_{C_{(2)}} \left(U_{G_3} \otimes U_{A_1}\right)^T, \tag{36}$$

$$A_{C_{(3)}} = U_{G_3} S_{C_{(3)}} \left(U_{A_2} \otimes U_{A_1}\right)^T. \tag{37}$$

By separating the frontal slices $A_{C_i}, i = 1, 2, 3, 4$ from tensor $\mathcal{A}_{\mathcal{C}}$, we obtain the following compensation wavelet subbands:

$$LL_C = A_{C_1}, HL_C = A_{C_2}, LH_C = A_{C_3}, HH_C = A_{C_4}. \tag{38}$$

The image is reconstructed by applying 2D-i DWT to obtain the compensated image. Fig. 4(a)–(d) illustrate the results of using the proposed method in the FVC 2002 and NIST-4 fingerprint databases. As displayed in Fig. 4, this method can effectively remove the background and blurred regions to provide an image exhibiting a near-normal distribution. In addition, the proposed method enhances the clarity and continuity of ridge structures in fingerprint images.

The purpose of this study is to obtain an enhanced fingerprint image that exhibited a normal distribution. The Daubechies wavelet is employed because of its compactness. To reduce the complexity and time of computation, the first-level coarse resolution is adopted in the experiments. If the image is too dark, the compensation coefficient is increased, whereas if the image is too light, the compensation coefficient is decreased. Because the dynamic scope of pixel values is between 0 and 255, the mean and standard values of the normal distribution are 128 and the square root of 32, respectively. An increase in the mean value increases the singular value of the Gaussian template and the compensation coefficient. Most of the fingerprint images are low in contrast

and too dark. Thus, the images have low means and singular values in all subbands after the application of DWT and HOSVD. Therefore, we employ a Gaussian template with a higher mean than usual to increase the compensation coefficient. If the image is too dark, the compensation coefficient is higher than 1. If the image is too light, the compensation coefficient is lower than 1. Our observations in both the NIST-4 and FVC 2002 databases showed that the optimal method is to set the mean value of the Gaussian template to 208 and the standard deviation to the square root of 32. The framework of the proposed method, named adaptive higher-order singular value decomposition on a tensor of wavelet subbands of a fingerprint (AHTWF), is summarized in Algorithm 1.

Algorithm 1 AHTWF Method

Input: Fingerprint image f of size $2M \times 2N$

Output: Fingerprint image obtained after using the AHTWF method

1. Construct a Gaussian template Ga of size $2M \times 2N$.
2. Apply 2D-DWT at scale level 1 for f and Ga to obtain the frequency subband coefficients.
3. Construct wavelet subband tensor $\mathcal{A}, \mathcal{G} \in \mathbb{R}^{M \times N \times 4}$ space (Fig. 2).
4. Calculate the maxima of all coefficients for each frontal slice of $\mathcal{A}$ and $\mathcal{G}$ by using Eqs.(19) and (20), respectively.
5. Calculate the HOSVD of $\mathcal{A}$ and $\mathcal{G}$ by using Eqs.(21)–(27).
6. Calculate the maxima of all coefficients for each frontal slice of core $\mathcal{S}$ of $\mathcal{A}$ and core $\mathcal{C}$ of $\mathcal{G}$ by using Eqs.(28) and (29), respectively.
7. Calculate the compensation weight coefficients by using Eqs. (30)–(33).
8. Update the frontal slices of core $\mathcal{S}$ of $\mathcal{A}$ by using Eq.(34).
9. Update the frequency subband coefficients by using Eqs. (35) - (37) to obtain the compensated frequency subband coefficients.
10. Reconstruct the compensated subbands to obtain the AHTWF image by applying 2D-i DWT to the compensated frequency subbands.

V. EXPERIMENTAL RESULTS AND DISCUSSION

The HOSVD decomposes the tensor into four main components includes the core tensor and three types of inverse factors. These components contain specific information on data within the tensor. Besides, the core tensor contains the frontal slices where each of the frontal slices also contains more detail information, as discussed more detail in Section III.B. The wavelet transform can decompose the fingerprint image into 4 subbands that contain specific information. However, the change of these subbands to enhance the fingerprint image is not enough. Wang *et al.* [19] proposed the method based on SVD to find the linear relation between wavelet subbands and compute the compensation coefficients to enhance the fingerprint image. This method is limited to finding the relation among wavelet subbands in only one direction. By constructing the tensor of wavelet subbands of the fingerprint image and using the HOSVD to decompose it into more detail components, we can find more information and the relation of wavelet subbands in three directions. Thus, our proposed method gets better results comparing previous fingerprint image enhancement methods. Moreover, the compensation weight coefficients of each frontal slice are calculated based on the tensor of the fingerprint image wavelet subbands and the corresponding tensor of the Gaussian template image wavelet subbands. The order of wavelet subbands in the tensor does not affect the final result. Besides, the compensation weight coefficients are calculated automatically without a threshold and the fingerprint contrast is adaptively adjusted by multiplying the frontal slices of core tensor with the corresponding compensation coefficients. Thus, our proposed method enhances the fingerprint adaptively and gets better results in comparison with the previous fingerprint image enhancement methods.

To demonstrate the efficiency of the proposed method, we compared the results obtained using the proposed method with those obtained using related methods, including histogram equalization (HE) [34], Sharma and Dey [11], and the method of Wang *et al.* [19]. Experiments were performed using multiple fingerprint databases, including FVC 2002 and NIST-4. NIST-4 is a key benchmark for fingerprint classification. Most related published results are in this database. Thus, for comparison with other approaches, we applied our fingerprint classification algorithm in NIST-4, which contains 4000 ink-on-paper fingerprint images of size 512×512 pixels taken from 2000 fingers with two instances per finger. The first fingerprint instances are numbered f0001 to f2000, and the second instances are numbered s0001 to s2000. The Arch, Tented Arch, Left Loop, Right Loop, and Whorl classes are evenly distributed throughout the database. Each fingerprint in NIST-4 has been assigned to one or two of the five classes by experts. There exist approximately 17% ambiguous fingerprints that have two classes assigned to them. FVC 2002 includes four databases, namely DB1, DB2, DB3, and DB4, which are compiled using multiple sensors and technologies that are widely used. Each database has a width (w) of 110 fingers and depth (d) of eight impressions per finger (880 fingerprints in total). Fingers 101 to 110 (set B) were made available to the participants to allow for parameter tuning before the submission of the algorithms. The benchmark was then set on the basis of fingers 1 to 100 (set A). Volunteers were randomly divided into three groups (30 volunteers per group), and each group was assigned to one database and therefore to a different fingerprint scanner. Each volunteer was invited to present himself or herself at the collection point for three distinct sessions, with at least 2 weeks between each session. The forefinger and middle finger of both hands (four fingers in total) of each volunteer were imaged by interleaving the fingers to

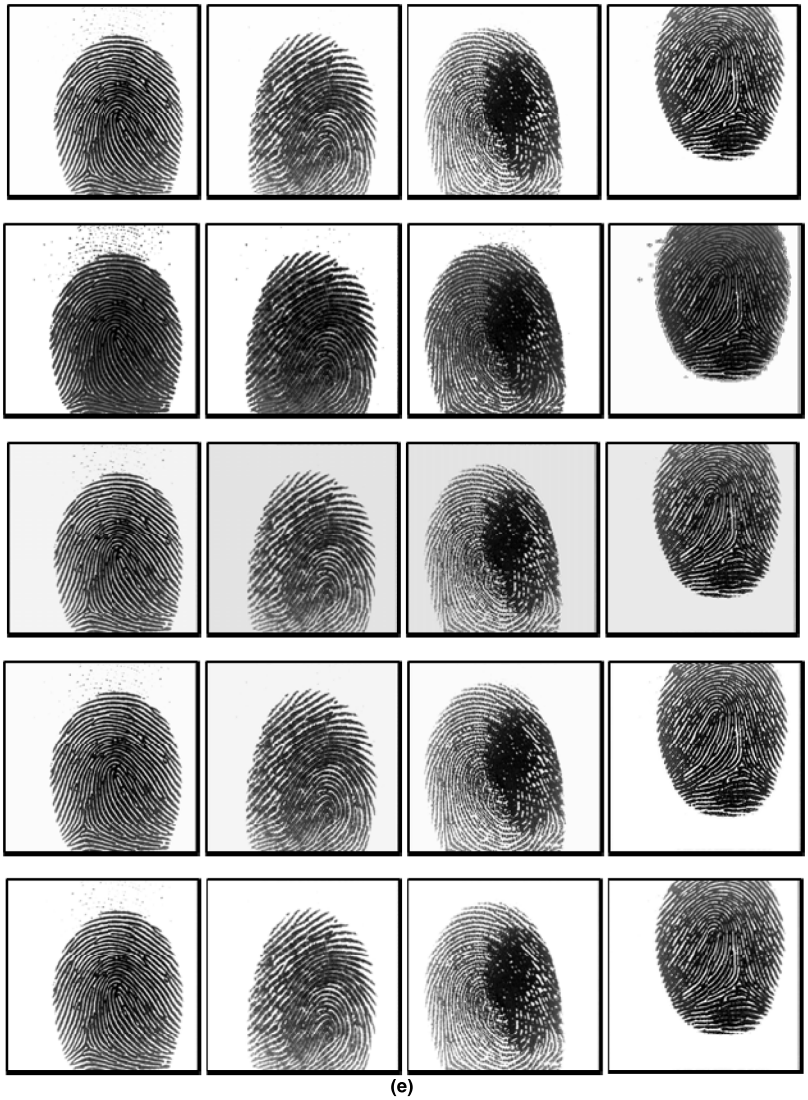

FIGURE 5. Some samples results of different enhancement approach on FVC2002 DB1-A fingerprint database. (a) The original images. (b) HE images. (c) Sharma and Dey method. (d) Wang et al. method. (e) Our proposed method.

maximize the differences in finger placement. No efforts were made to control the image quality, and the sensor platens were not systematically cleaned. In each session, four impressions were acquired from each of the four fingers per volunteer. During the second session, the volunteers were requested to exaggerate the displacement (impressions 1 and 2) and rotation (impressions 3 and 4) of each finger without exceeding 35°. During the third session, the fingers were alternately dried (impressions 1 and 2) and moistened (impressions 3 and 4).

Fig. 5 shows some images from FVC 2002 DB1-A and Fig. 6 displays some images from FVC 2002 DB2-A. Fig. 7 illustrates some images from NIST-4 and enhancement images obtained after using HE [34], Sharma and Dey [11], Wang *et al.* [19], and the proposed method. The results show that the enhanced fingerprint images by the proposed algorithm have better quality in comparison with the other method. Not only the enhanced fingerprint image can improve the clarity and continuity of ridge structures, but can also remove the background of a fingerprint image.

To demonstrate the usefulness of the proposed algorithm, we evaluated its fingerprint classification performance by applying the classification flowchart in [2] to the compensated fingerprint images. The compensation results of the proposed method were then compared with those of the original images. Wang [2] first calculated the singular point of a fingerprint image by applying the adaptive Poincare index method and then used the number of singular points and the traced orientation field flow to classify fingerprints into seven classes. Arch (A), Tented Arch (T), Left loop (L), Right loop (R), and Whorl (W) are well-known

FIGURE 6. Some samples results of different enhancement approach on FVC2002 DB2-A fingerprint database. (a) The original images. (b) HE images. (c) Sharma and Dey method. (d) Wang et al. method. (e) Our proposed method.

fingerprint types defined in the Henry system. The other two types, namely Eddy (E) and S-type (S), were classified under Whorl. Fig. 8 displays an accurate example of the seven fingerprint classes when the traced orientation field flow is obtained using the proposed method. Notably, the classification method based on the number of singular points and the traced orientation field flow is highly sensitive to the fingerprint quality. Therefore, if the quality of a fingerprint image is high, the classification rate is also high.

We compare the compensated image with the original image. In the experiments, 2000 fingerprint images numbered s0001 to s2000 from NIST-4 and all fingerprint images from FVC 2002 DB1-A and DB2-A were selected. Because the W, E, and S fingerprint classes overlap considerably, separating these three classes is extremely difficult. This difficulty also arises when the fingerprint classes A and T are considered. Therefore, to obtain six classes, the S and E classes were merged to create class E. To compare the classification results of the five classes, three classes—W, E, and S—were merged into one class, namely class W. In addition, the results of the four-class classification problem were obtained. Classes A and T were merged into one class, namely class A. The confusion matrices for the seven-class problem in NIST-4, FVC 2002 DB1-A, and FVC 2002 DB2-A are presented in Tables 1, 2, and 3, respectively.

TABLE 1. Confusion matrix for 7-classes of NIST-4 database.

Hypothesized class	True class						
	A	T	L	R	W	S	E
A	436	1	3	5	0	0	0
T	7	317	6	1	1	0	0
L	2	2	414	0	0	2	0
R	0	4	2	435	1	1	0
W	0	0	3	1	87	4	0
S	0	0	0	0	0	76	1
E	0	0	3	2	2	8	173

TABLE 2. Confusion matrix for 7-classes oF FVC2002 DB1-A database.

Hypothesized class	True class						
	A	T	L	R	W	S	E
A	24	1	1	1	0	0	0
T	0	28	2	1	0	0	0
L	1	2	279	2	0	1	0
R	1	0	1	297	0	2	0
W	0	1	2	5	49	0	2
S	0	0	0	0	0	24	0
E	0	0	3	6	1	1	62

TABLE 3. Confusion matrix for 7-classes of FVC2002 DB-A database.

Hypothesized class	True class						
	A	T	L	R	W	S	E
A	41	1	3	1	0	0	1
T	2	29	3	1	0	2	0
L	1	0	288	2	0	1	1
R	0	0	2	258	0	1	0
W	0	0	1	3	72	0	2
S	0	0	0	1	0	18	0
E	0	0	1	2	1	0	61

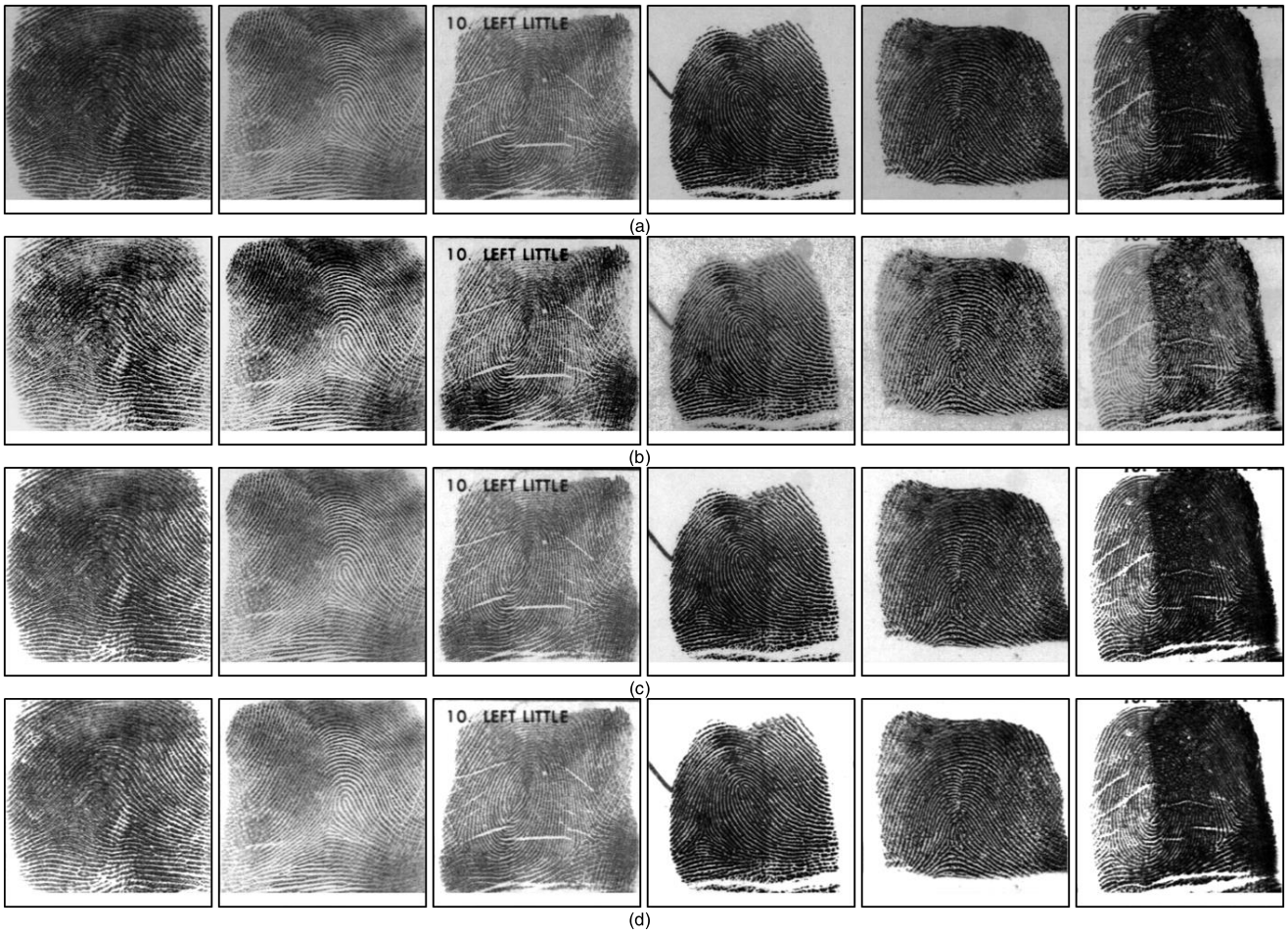

FIGURE 7. Sample results of enhancement approaches in the NIST-4 fingerprint database. (a) Original images and images obtained when using (b) HE, (c) the method of Wang et al., and (d) the proposed method.

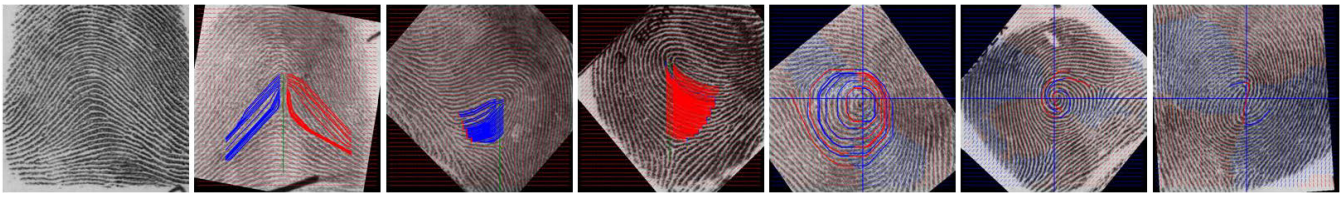

FIGURE 8. 7-class fingerprint examplesof NIST-4 obtained with the proposed method and [2].

The performance of a fingerprint classification algorithm is measured according to the degree of accuracy throughout the testing set, which is defined as the percentage of accurate classification. We compared our method with several modern techniques introduced in [3]–[5], [7], [11] and [19]. In addition to the classification results for the seven classes in our system, those for the sets of our and five classes are reported in Table 4. As presented in this table, Cao *et al.* [3] proposed a regularized orientation diffusion model for fingerprint orientation extraction and a hierarchical classifier for fingerprint classification. They obtained classification accuracies of 95.90% and 97.20%. Liu [4] used the Adaboost learning method to model multiple singularity features and obtained accuracies of 94.10% and 95.70%. Li *et al.* [5] used coefficients of an orientation model for fingerprint classification and obtained accuracy rates of 93.50% and 95%. Using the classification method [2] for the enhanced fingerprint images by Sharma and Dey method [11] on FVC02 DB1-A, we achieved classification accuracies of 94.5%, 95.12%, 95.25%, and 95.30% for the seven-, six-, five- and four-class problems. Jain *et al.* [7] proposed the Gabor filter and two-stage classifier for fingerprint classification. In their

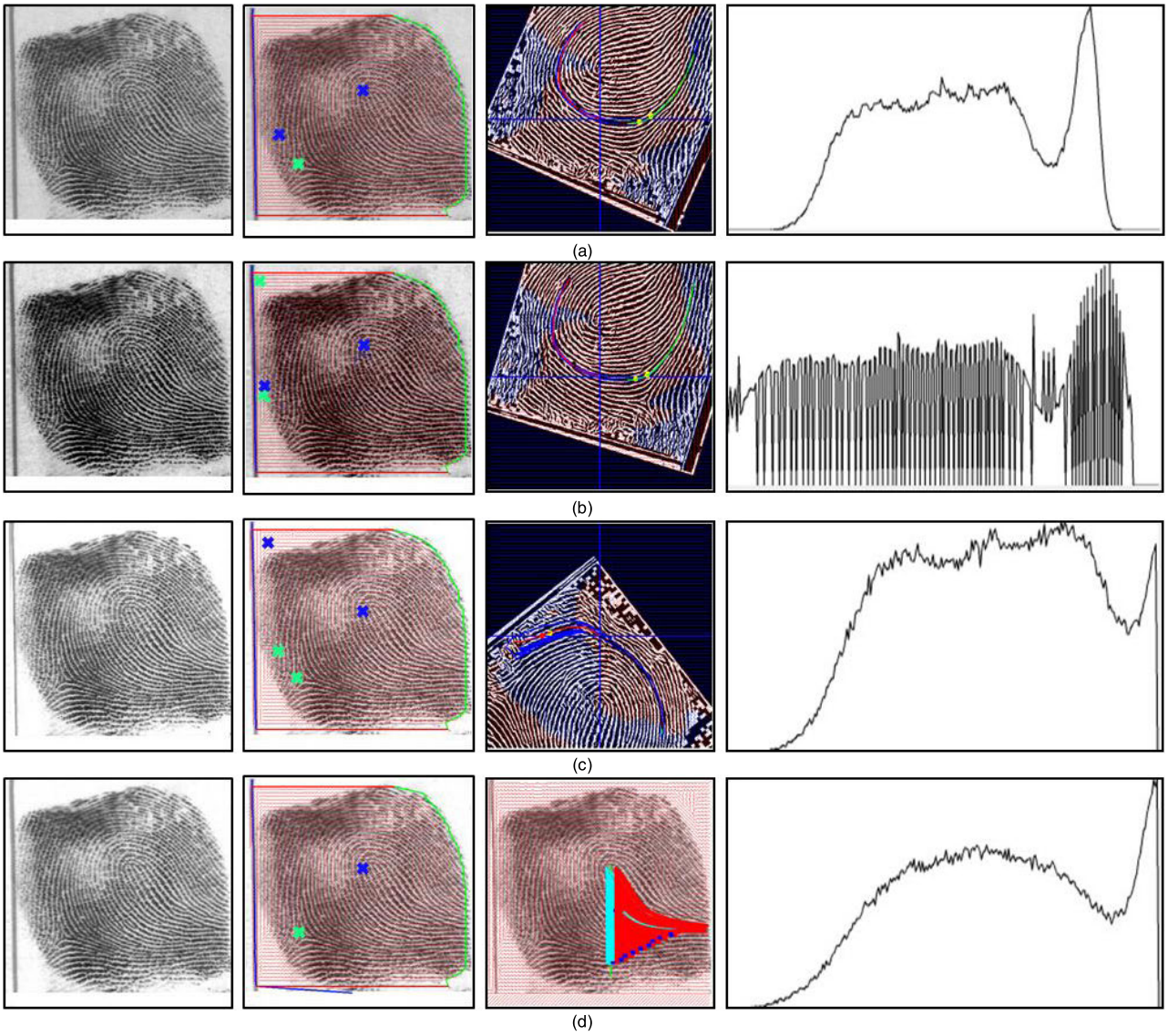

FIGURE 9. An example of misclassified on the original image and truly classified on the compensated image. From left to right on each row: The fingerprint image, the orientation field and result on singular point detection image (core point in blue mark and the delta point in green mark), the classification results and fingerprint image histogram. (a) Original image classified as E type. (b) HE image classified as E type. (c) Wang's image classified as E type. (d) Our method image with true classification.

method, the first stage uses a K-nearest neighbor classifier to find the two most probable classes and the second stage uses a neural network for the final decision. Classification rates of 90.00% and 95.80% were obtained for problems with four and five classes, respectively. Wang *et al.* [19] first used a novel lighting compensation scheme involving adaptive SVD on wavelet coefficients to enhance fingerprint images and then classified the fingerprint according to the number of singular points and the traced orientation field flow. NIST-4 accuracy rates of 94.75%, 95.45%, 96.55%, and 97.35% were obtained for problems with seven-, six-, five-, and four-classes, respectively. They achieved five-classes accuracy rates with 95.25% for FVC 2002 DB1-A and 95.12% for FVC 2002 DB2-A. Furthermore, they achieved 95.12%, 95.25%, and 95.36% accuracy and 95%, 95%, and 95.75% accuracy for the seven-, six- and four-classes problems in FVC 2002 DB1-A, and FVC 2002 DB2-A, respectively. The proposed method achieved classification accuracies of 96.90%, 97.35%, 97.65%, and 98.05% for the seven-,six-, five- and four-class problems in the NIST-4 database. In addition, the method obtained 95.38%, 95.50%, 95.63%, and 95.75% accuracy and 95.88%, 95.88%, 96.25%, and 96.63% accuracy for the seven-, six-, five-, and four-class problems in FVC 2002 DB1-A and FVC 2002 DB2-A, respectively. These results revealed that our system can achieve high accuracy in sets of not only four and five classes but also six and seven classes. Thus, the proposed method is a pioneering system for classifying Whorl, S-type, and Eddy fingerprints.

TABLE 4. Accuracy of various fingerprint classification approaches on NIST-4 and FVC-2002 databases.

Algorithm	7-class (%)	6-class (%)	5-class (%)	4-class (%)	Data set
Cao *et al.* [3]	*	*	95.90	97.20	NIST-4 2ndhalf
Liu [4]	*	*	94.10	95.70	NIST-4 2ndhalf
Li *et al.* [5]	*	*	93.50	95.00	NIST-4 2ndhalf
Jain *et al.* [7]	*	*	90.00	95.80	NIST-4 2ndhalf
Wang [2] withSharma and Dey [11]	94.5	95.12	95.25	95.30	FVC02 DB1-A
Wang *et al.* [19]	94.75	95.45	96.55	97.35	NIST-4 2ndhalf
	95.12	95.25	95.25	95.36	FVC02 DB1-A
	95.00	95.00	95.12	95.75	FVC02 DB2-A
Wang [2] with the proposed method	**96.90**	**97.35**	**97.65**	**98.05**	NIST-4 2ndhalf
	95.38	**95.50**	**95.63**	**95.75**	FVC02 DB1-A
	95.88	**95.88**	**96.25**	**96.63**	FVC02 DB1-A

VI. CONCLUSION

The performance of a fingerprint classification system relies considerably on the fingerprint image quality. However, satisfactory image quality is difficult to obtain in reality. To overcome this problem, a novel fingerprint enhancement algorithm that can considerably enhance the clarity and continuity of ridge structures is proposed in this paper. This algorithm effectively removes the backgrounds and blurred regions of fingerprint images. In addition, the proposed method effectively improves the quality of fingerprint images and therefore increases the accuracy of fingerprint classification.

REFERENCES

[1] E. R. Henry, *Classification and uses of Finger Prints*. London, U.K.: George Rutledge & Sons, 1900.
[2] J.-W. Wang, "Classification of fingerprint based on traced orientation flow," in *Proc. IEEE Int. Symp. Ind. Electron.*, Bari, Italy, Jul. 2010, pp. 1585–1588.
[3] K. Cao, L. Pang, J. Liang, and J. Tian, "Fingerprint classification by a hierarchical classifier," *Pattern Recognit.*, vol. 46, no. 12, pp. 3186–3197, Dec. 2013.
[4] M. Liu, "Fingerprint classification based on Adaboost learning from singularity features," *Pattern Recognit.*, vol. 43, no. 3, pp. 1062–1070, Mar. 2010.
[5] J. Li, W.-Y. Yau, and H. Wang, "Combining singular points and orientation image information for fingerprint classification," *Pattern Recognit.*, vol. 41, no. 1, pp. 353–366, Jan. 2008.
[6] R. Cappelli, D. Maio, D. Maltoni, and L. Nanni, "A two-stage fingerprint classification system," in *Proc. ACM SIGMM Workshop Biometrics Methods Appl. (WBMA)*, 2003, pp. 95–99.
[7] A. Jain, S. Prabhakar, and L. Hong, "A multichannel approach to fingerprint classification," *IEEE Trans. Pattern Anal. Mach. Intell.*, vol. 21, no. 4, pp. 348–359, Apr. 1999.
[8] S. Wang and Y. Wang, "Fingerprint enhancement in the singular point area," *IEEE Signal Process. Lett.*, vol. 11, no. 1, pp. 16–19, Jan. 2004.
[9] W. Wang, J. Li, F. Huang, and H. Feng, "Design and implementation of Log–Gabor filter in fingerprint image enhancement," *Pattern Recognit. Lett.*, vol. 29, no. 3, pp. 301–308, Feb. 2008.
[10] C. Gottschlich, "Curved-region-based ridge frequency estimation and curved Gabor filters for fingerprint image enhancement," *IEEE Trans. Image Process.*, vol. 21, no. 4, pp. 2220–2227, Apr. 2012.
[11] R. P. Sharma and S. Dey, "Two-stage quality adaptive fingerprint image enhancement using fuzzy C-means clustering based fingerprint quality analysis," *Image Vis. Comput.*, vols. 83–84, pp. 1–16, Mar. 2019.
[12] S. Jirachaweng, Z. Hou, W.-Y. Yau, and V. Areekul, "Residual orientation modeling for fingerprint enhancement and singular point detection," *Pattern Recognit.*, vol. 44, no. 2, pp. 431–442, Feb. 2011.
[13] E.-K. Yun and S.-B. Cho, "Adaptive fingerprint image enhancement with fingerprint image quality analysis," *Image Vis. Comput.*, vol. 24, no. 1, pp. 101–110, Jan. 2006.
[14] K. Cao and A. K. Jain, "Learning fingerprint reconstruction: From minutiae to image," *IEEE Trans. Inf. Forensics Security*, vol. 10, no. 1, pp. 104–117, Jan. 2015.
[15] H. Fronthaler, K. Kollreider, and J. Bigun, "Local features for enhancement and minutiae extraction in fingerprints," *IEEE Trans. Image Process.*, vol. 17, no. 3, pp. 354–363, Mar. 2008.
[16] J. Lei, H. Hatem, L. Zhou, X. You, P. S. P. Wang, and D. Xu, "Fingerprint enhancement based on non-separable wavelet," in *Proc. 9th IEEE Int. Conf. Cogn. Informat. (ICCI)*, Jul. 2010.
[17] C.-T. Hsieh, E. Lai, and Y.-C. Wang, "An effective algorithm for fingerprint image enhancement based on wavelet transform," *Pattern Recognit.*, vol. 36, no. 2, pp. 303–312, Feb. 2003.
[18] D. Bennet and S. A. Perumal, "Fingerprint: DWT, SVD based enhancement and significant contrast for ridges and valleys using fuzzy measures," *J. Comput. Sci. Eng.*, vol. 6, no. 1, pp. 28–32, 2011.
[19] J.-W. Wang, N. Tuyen Le, C.-C. Wang, and J.-S. Lee, "Enhanced ridge structure for improving fingerprint image quality based on a wavelet domain," *IEEE Signal Process. Lett.*, vol. 22, no. 4, pp. 390–394, Apr. 2015.
[20] L. R. Tucker, "Implications of factor analysis of three-way matrices for measurement of change," in *Problems in Measuring Change*, C. W. Harris, Ed. Madison, WI, USA: Univ. Wisconsin Press, pp. 122–137, 1963.
[21] L. R. Tucker, "The extension of factor analysis to three-dimensional matrices," in *Contributions to Mathematical Psychology*. New York, NY, USA: Holt, Rinehart and Winston, 1963, pp. 109–127.
[22] L. R. Tucker, "Some mathematical notes on three-mode factor analysis," *Psychometrika*, vol. 31, no. 3, pp. 279–311, Sep. 1966.
[23] L. Omberg, G. H. Golub, and O. Alter, "A tensor higher-order singular value decomposition for integrative analysis of DNA microarray data from different studies," *Proc. Nat. Acad. Sci. USA*, vol. 104, no. 47, pp. 18371–18376, Nov. 2007.
[24] L. Omberg, J. R. Meyerson, K. Kobayashi, L. S. Drury, J. F. X. Diffley, and O. Alter, "Global effects of DNA replication and DNA replication origin activity on eukaryotic gene expression," *Mol. Syst. Biol.*, vol. 5, no. 1, p. 312, Jan. 2009.
[25] C. Muralidhara, A. M. Gross, R. R. Gutell, and O. Alter, "Tensor decomposition reveals concurrent evolutionary convergences and divergences and correlations with structural motifs in ribosomal RNA," *PLoS ONE*, vol. 6, no. 4, Apr. 2011, Art. no. e18768.
[26] M. A. O. Vasilescu and D. Terzopoulos, "TensorTextures: Multilinear image-based rendering," in *Proc. ACM SIGGRAPH Papers*, Los Angeles, CA, USA, Aug. 2004, pp. 336–342.
[27] M. A. O. Vasilescu and D. Terzopoulos, "Multilinear subspace analysis of image ensembles," in *Proc. Comput. Vis. Pattern Recognit. (CVPR)*, Madison, WI, USA, vol. 2, Jun. 2003, pp. 93–99.
[28] M. A. O. Vasilescu and D. Terzopoulos, "Multilinear analysis of image ensembles: Tensorfaces," in *Proc. 7th Eur. Conf. Comput. Vis. (ECCV)*, Copenhagen, Denmark, May 2002, pp. 447–460.
[29] H.-S. Lee and D. Kim, "Tensor–based AAM with continuous variation estimation: Application to variation–robust face recognition," *IEEE Trans. Pattern Anal. Mach. Intell.*, vol. 31, no. 6, pp. 1102–1116, Jun. 2009.
[30] K. Jia and S. Gong, "Generalized face super–resolution," *IEEE Trans. Image Process.*, vol. 17, no. 6, pp. 873–886, Jun. 2008.
[31] S.-J. Wang, J. Yang, N. Zhang, and C.-G. Zhou, "Tensor discriminant color space for face recognition," *IEEE Trans. Image Process.*, vol. 20, no. 9, pp. 2490–2501, Sep. 2011.
[32] C. I. Watson and C. L. Wilson, "NIST special database 4: NIST 8-bit gray scale images of fingerprint image groups (FIGS)," Nat. Inst. Standards Technol., Gaithersburg, MD, USA, Interagency Rep. 8210, 1992.
[33] D. Maio, D. Maltoni, R. Cappelli, J. Wayman, and A. Jain, "FVC2002: Second fingerprint verification competition," in *Proc. Object Recognit. Supported User Interact. Service Robots*, vol. 3, Jun. 2003, pp. 811–814.
[34] R. C. Gonzalez and R. E. Wood, *Digital Image Processing*, 3rd ed. Upper Saddle River, NJ, USA: Prentice-Hall, 2007.
[35] S. G. Mallat, "A theory for multiresolution signal decomposition: The wavelet representation," *IEEE Trans. Pattern Anal. Mach. Intell.*, vol. 11, no. 7, pp. 674–693, Jul. 1989.
[36] T. G. Kolda and B. W. Bader, "Tensor decompositions and applications," *SIAM Rev.*, vol. 51, no. 3, pp. 455–500, Aug. 2009.

NGOC TUYEN LE received the B.S. degree in mathematics and information from the Hanoi National University of Education, Hanoi, Vietnam, in 1996, the M.S. degree in computer science from Le Qui Don Technical University, Hanoi, Vietnam, in 2006, and the Ph.D. degree in electronic engineering from the National Kaohsiung University of Science and Technology, Taiwan, in 2015. He is currently a Postdoctoral Researcher with the Institute of Photonics Engineering, National Kaohsiung University of Science and Technology, Taiwan. His research interests include digital image processing, automatic optical inspection system, face recognition, and fingerprint classification.

JING-WEIN WANG received the B.S. and M.S. degrees in electrical engineering from the National Taiwan University of Science and Technology, in 1986 and 1988, respectively, and the Ph.D. degree in electrical engineering from National Cheng Kung University, Taiwan, in 1998. He was the Chief Project Leader with the Equipment Design Center of PHILIPS, Taiwan, from 1992 to 2000. In 2000, he joined the faculty of the National Kaohsiung University of Science and Technology as the Dean of the College of Electrical Engineering and Information Science. He is currently a Distinguished Professor with the Institute of Photonics Engineering. His current research interests include combinatorial optimization, pattern recognition, and wavelets and their applications.

DUC HUY LE received the B.Sc. degree in computer science from the Hanoi University of Industry, Hanoi, Vietnam, in 2012, and the M.Sc. degree from the National Kaohsiung University of Applied Sciences, Kaohsiung, Taiwan, in 2015. He is currently pursuing the Ph.D. degree with the Department of Electronic Engineering, National Kaohsiung University of Science and Technology. His current research interests include digital image processing, face recognition, and image enhancement.

CHIH-CHIANG WANG received the Ph.D. degree in computer science from North Carolina State University, Raleigh, NC, USA, in 2007. He is currently a Faculty Member with the Department of Computer Science and Information Engineering, National Kaohsiung University of Science and Technology, Taiwan. His research interests include the broad fields of computer networking, tensors, and cloud/edge computation systems.

TU N. NGUYEN (Senior Member, IEEE) received the Ph.D. degree in electronic engineering from the National Kaohsiung University of Science and Technology (formerly, National Kaohsiung University of Applied Sciences), in 2016. He joined the Missouri University of Science and Technology as a Postdoctoral Researcher with the Intelligent Systems Center, in 2016. He was a Postdoctoral Associate with the Department of Computer Science and Engineering, University of Minnesota–Twin Cities, in 2017. He is currently an Assistant Professor with the Department of Computer Science, Purdue University Fort Wayne. His research interests include design and analysis of algorithms, network science, cyber-physical systems, and cybersecurity. He has served as a Technical Program Committee Member for over 50 premium conferences in the areas of network and communication, such as INFOCOM, Globecom, ICC, and RFID. He has served as the Technical Program Committee Chair for the NICS 2019, SoftCOM (25th) and ICCASA 2017, the Publicity Chair for iCAST 2017 and BigDataSecurity 2017, and the Track Chair for ACT 2017. He has been serves as an Associate Editor for the *EURASIP Journal on Wireless Communications and Networking*, since 2017. Since 2017, he has also been on the Editorial Board of the *Cybersecurity Journal* and *Internet Technology Letters*, the *International Journal of Vehicle Information and Communication Systems*, the *International Journal of Intelligent Systems Design and Computing*, and *IET Wireless Sensor Systems*.